



Published in final edited form as:

*J Magn Reson Imaging*. 2019 May ; 49(5): 1475–1488. doi:10.1002/jmri.26325.

## Ultrashort Echo Time Imaging for Quantification of Hepatic Iron Overload: Comparison of Acquisition and Fitting Methods via Simulations, Phantoms, and In vivo Data

Aaryani Tipirneni-Sajja<sup>1</sup>, Ralf B. Loeffler<sup>1</sup>, Axel J. Krafft<sup>1,2</sup>, Andrea N. Sajewski<sup>1</sup>, Robert J. Ogg<sup>1</sup>, Jane S. Hankins<sup>3</sup>, Claudia M. Hillenbrand<sup>1</sup>

<sup>1</sup>Department of Diagnostic Imaging, St. Jude Children's Research Hospital, Memphis, TN, USA.

<sup>2</sup>Department of Radiology, Medical Physics, Medical Center–University of Freiburg, Faculty of Medicine, University of Freiburg, Freiburg, Germany.

<sup>3</sup>Department of Hematology, St. Jude Children's Research Hospital, Memphis, TN, USA.

### Abstract

**BACKGROUND:** Current R2\*-MRI techniques for measuring hepatic iron content (HIC) use various acquisition types and fitting models.

**PURPOSE:** To evaluate accuracy and precision of R2\*-HIC acquisition and fitting methods.

**STUDY TYPE:** Signal simulations, phantom study, and prospective *in-vivo* cohort.

**POPULATION:** 132 patients (58/74 male/female, mean age 17.7y).

**FIELD STRENGTH/SEQUENCE:** 2D-multi-echo gradient-echo (GRE) and ultra-short echo time (UTE) acquisitions at 1.5T.

**ASSESSMENT:** Synthetic MR signals were created to mimic published GRE and UTE methods, using different R2\* values (25–2000s<sup>-1</sup>) and signal-to-noise ratios (SNR). Phantoms with varying iron concentrations were scanned at 1.5T. *In-vivo* data were analyzed from 132 patients acquired at 1.5T. R2\* was estimated by fitting using three signal models. Accuracy and precision of R2\* measurements for UTE acquisition parameters (SNR, echo spacing (TE), maximum echo time (TE<sub>max</sub>)) and fitting methods were compared for simulated, phantom, and *in-vivo* datasets.

**STATISTICAL TESTS:** R2\* accuracy was determined from the relative error and by linear regression analysis. Precision was evaluated using coefficient of variation (CoV) analysis.

**RESULTS:** In simulations, all models had high R2\* accuracy (error<5%) and precision (CoV<10%) for all SNRs, shorter TE (0.5ms) and longer TE<sub>max</sub> (10.1ms); except the constant offset model overestimated R2\* at the lowest SNR. In phantoms and *in-vivo*, all models produced similar R2\* values for different SNRs and shorter TEs (slopes: 0.99–1.06, R<sup>2</sup>>0.99, P<0.001). In

**Correspondence to:** Claudia M. Hillenbrand, PhD, Department of Diagnostic Imaging, St. Jude Children's Research Hospital, 262 Danny Thomas Place, Memphis, TN 38105-3678, USA, Phone: 901-595-4118, Fax: 901-595-3981, claudia.hillenbrand@stjude.org.

Disclosure:

This work will be presented in part at the 2018 Annual Meeting of the International Society of Magnetic Resonance in Medicine in Paris, France.

all experiments,  $R2^*$  results degraded for high  $R2^*$  values with longer  $TE$  ( $> 1$  ms). *In-vivo*, shorter and longer  $TE_{max}$  gave similar  $R2^*$  results (slopes: 1.02–1.06,  $R^2 > 0.99$ ,  $P < 0.001$ ) for the noise subtraction model for  $25 < R2^* < 2000$  s $^{-1}$ . However, both quadratic and constant offset models, using shorter  $TE_{max}$  ( $< 4.7$  ms) overestimated  $R2^*$  and yielded high CoVs up to  $\sim 170\%$  for low  $R2^*$  ( $< 250$  s $^{-1}$ ).

**DATA CONCLUSION:** UTE with  $TE_{max} = 10.1$  ms and  $TE = 0.5$  ms yields accurate  $R2^*$  estimates over the entire clinical HIC range. Mono-exponential fitting with noise subtraction is the most robust signal model to changes in UTE parameters and achieves the highest  $R2^*$  accuracy and precision.

## Keywords

hepatic iron overload;  $R2^*$  quantification; ultrashort echo time; signal models

## INTRODUCTION

Hepatic iron overload is a severe complication in patients with increased gastrointestinal absorption of dietary iron or those receiving chronic blood transfusions.<sup>1–5</sup> Measuring and monitoring hepatic iron content (HIC) is thus necessary to guide treatment for removing excess iron. In recent years, magnetic resonance imaging (MRI) has become accepted as a reliable tool to estimate HIC.<sup>6</sup> One standard method to estimate HIC with MRI is to quantify the effective transverse relaxation rate ( $R2^*$ ) of liver tissue using a multi-echo gradient echo (GRE) sequence. Published calibration studies show excellent linear correlation between HIC by biopsy and  $R2^*$  measured by GRE.<sup>7–10</sup> However, in cases of high and massive iron overload (HICs  $> 15$  and  $25$  mg/g Fe dry weight liver tissue, respectively), precision of GRE-based HIC is limited and  $R2^*$  estimation may fail, as the signal decays too rapidly to be reliably measured by conventional GRE imaging with shortest possible echo times of  $\sim 1.0$  ms.<sup>7</sup>

Recently, independent groups have shown that ultrashort echo time (UTE) imaging with  $TE$  as short as  $0.1$ – $0.19$  ms can increase the accuracy of  $R2^*$  measurements in cases of high and massive iron overload,<sup>11,12</sup> and hence may extend the clinically measurable  $R2^*$ -MRI based HIC range. However, these groups use different UTE acquisition sequences, imaging parameters and  $R2^*$  fitting models,<sup>11,12</sup> and thus may produce different  $R2^*$  values and ultimately different  $R2^*$ -HIC calibrations, similar to the inconsistencies observed between previous GRE calibration studies.<sup>7–10</sup> The purpose of this study is, therefore, to evaluate accuracy and precision of  $R2^*$  acquisition and fitting methods of (a) previously published  $R2^*$ -GRE biopsy calibration studies, and (b) currently investigated  $R2^*$ -UTE methods, through simulations and measurements in phantoms and patients with hepatic iron overload.

## METHODS

### Simulations

Simulations were performed for the following published GRE and UTE acquisition and fitting methods: GRE-A,<sup>7</sup> GRE-B,<sup>8</sup> GRE-C,<sup>13</sup> UTE-A,<sup>11</sup> and UTE-B.<sup>12</sup> GRE-A acquires multiple single-echo GRE measurements from a single axial mid-hepatic slice and fits  $R2^*$

using a mono-exponential model with constant offset.<sup>7</sup> GRE-B acquires a multi-echo GRE sequence with bipolar readout gradients from a single axial central slice of the liver and fits  $R2^*$  using a mono-exponential model with noise subtraction.<sup>8</sup> GRE-C also uses a multi-echo GRE, it fits  $R2^*$  using a quadratic mono-exponential model.<sup>13</sup> UTE-A is implemented as a 2D multi-echo UTE with 5 interleaved echo trains with  $\Delta TE$  shifts of 0.25 ms to create denser sampling, and it fits  $R2^*$  using a quadratic mono-exponential model.<sup>11</sup> UTE-B acquires a 3D UTE sequence with 7 single-echoes and fits  $R2^*$  using a mono-exponential model with constant offset.<sup>12</sup> The acquisition parameters and signal models for all these methods are summarized in Table 1. Note that these 5 sequences have different acquisition times and echo time distributions. The simulation objective is to evaluate the precision and accuracy as a function of  $R2^*$  among the published, calibrated GRE and UTE  $R2^*$  methods. No emphasis on acquisition time is therefore made in the comparisons.

An analytical model was derived following an approach for optimized precision of T1 relaxation measurements,<sup>14</sup> to estimate the precision of fitted  $R2^*$  values<sup>15,16</sup> ( see also the Supplement for an analysis of the impact of key acquisition parameters on the precision of  $R2^*$  measurements). The precision of  $R2^*$  estimates calculated with different acquisition methods was compared by performing simulations in Maple (Maplesoft, Waterloo, ON) for different signal-to-noise ratio (SNR) conditions. SNR was defined as the ratio of the true signal intensity  $S(TE=0)$  to the noise standard deviation. For each acquisition type, independent of the signal model, the achievable precision, expressed as the coefficient of variation (CoV) = (standard deviation (SD) of  $R2^*$ )/(mean of  $R2^*$ ), was calculated from the Fisher information matrix of the model function (see Supplement for derivation).<sup>14</sup> For each acquisition type, independent of the signal model, the maximal achievable precision, expressed as the coefficient of variation (CoV) = (standard deviation (SD) of  $R2^*$ )/(mean of  $R2^*$ ), was calculated from the Fisher information matrix of the model function (see Supplement for derivation).<sup>14</sup> To compare the accuracy of  $R2^*$  measurements, Monte Carlo simulations were performed using MATLAB (MathWorks, Natick, MA) for the acquisition and signal models listed in Table 1 by varying SNR levels. Monte Carlo simulations were performed for 40  $R2^*$  values from 25 to 2000  $s^{-1}$  mimicking the range of iron overloaded liver tissue. Assuming normal distributed  $R2^*$  values in liver tissue, 10,000  $R2^*$  samples were drawn from a Gaussian distribution [mean = nominal  $R2^*$ , full width half maximum = 5% of the nominal  $R2^*$ ] for each nominal  $R2^*$  value, and a complex MR signal curve was generated using the reported TEs for each sequence type. Complex Gaussian noise was added to each synthetic signal to achieve the target SNR. The magnitude signal was subsequently fitted with the respective signal models to estimate  $R2^*$ .

The above two steps served to identify the most suited sequence amongst the 5 analyzed acquisition methods that demonstrated highest accuracy and precision over the widest range of  $R2^*$  values. For this sequence, further Monte Carlo simulations were performed to evaluate the performance of the reported  $R2^*$  signal models—constant offset,<sup>7,12</sup> noise subtraction,<sup>8,17</sup> and quadratic<sup>11,13</sup>—by varying the following sequence parameters: SNR (25, 50, 75 and 100),  $\Delta TE$  (echo spacing: 0.25, 0.5, 1.0 and 1.8 ms), and  $TE_{max}$  (maximum TE: 2.1, 4.7, 10.1 and 20.9 ms).

## Phantom Study

Ten phantoms (volume = 1 L) were made from 2% agar–water mixtures, doped with various amounts of bionized nonferrite particles (range of Fe concentration: 0.5 – 220 µg/ml) to obtain a wide range of  $R2^*$  values,<sup>17</sup> and scanned with a 1.5T scanner (Magnetom Avanto, Siemens Healthineers, Malvern, PA) using the following UTE-A acquisition parameters (see Table 1):TR/TE1, 52.5/0.1 ms; echo spacing, 1.8 ms; 12 echoes per interleave; 5 interleaves; 192 radial lines; flip angle, 20°; slice thickness, 10 mm; pixel bandwidth, 780 Hz/pixel; field of view (FOV) 420 mm and scan time, 60 seconds. For the UTE-A acquisition, two spatial saturation bands were placed parallel to the imaging slice (gap between saturation band and imaging slice, 10 mm; saturation band thickness, 100 mm) to eliminate out-of-slice signal contributions, and chemically selective saturation radiofrequency pulses were applied to reduce radial streaking artifacts. Images were acquired at different SNR by changing the number of averages (NA). SNR is calculated as the ratio of the mean signal intensity measured in the phantom to the SD of background noise. To investigate the impact of  $TE$  and  $TE_{max}$ , images at certain TEs were removed from the UTE-A acquisition for analysis. Quantitative  $R2^*$  maps were calculated in MATLAB from UTE-A data for the different signal models listed in Table 1 as a function of SNR,  $TE$ , and  $TE_{max}$ , similar to as performed in simulations. Circular regions of interest (ROIs) were drawn for each phantom bottle, and the mean ( $\pm$ SD)  $R2^*$  values for different signal models and acquisition parameters were calculated and compared.

## In vivo Study

DICOM and raw data were collected from patients who previously received more than 12 erythrocyte transfusions and provided consent, and enrolled in a prospective institutional review board–approved study on iron overload assessment ([www.clinicaltrials.gov](http://www.clinicaltrials.gov), NCT01572922). A total of 132 eligible patients (58 male and 74 female; mean [ $\pm$ SD] age, 17.7 $\pm$  11.5 years; range, 1.6–53.6 years) underwent a total of 137 MRI scans on a 1.5T scanner (Magnetom Avanto, Siemens Healthineers, Malvern, PA) from July 2012 to June 2017. Of these 43 were sedated (18 male and 25 female; mean [ $\pm$ SD] age, 7.6 $\pm$  5.8 years) for the MRI scan. Primary diagnoses included sickle cell disease ( $n=73$ ),  $\beta$ -thalassemia major ( $n=16$ ), cancer ( $n=27$ ), and other diseases (e.g., bone marrow failure syndromes, histiocytosis, pyruvate kinase deficiency) ( $n=16$ ).

A single transverse slice of the liver at the location of the main portal vein was scanned in all patients with the free-breathing UTE-A sequence which had identical parameters as the phantom study (see Table 1). The FOV for all acquisitions ranged from 350 to 500 mm depending on patient body size. To acquire images with high SNR, the UTE-A sequence was run with 3 averages instead of 1 as reported in Table 1. Quantitative  $R2^*$  maps were calculated in Matlab by fitting the signal decay on a pixel-by-pixel basis to different signal models given in Table 1.  $R2^*$  maps were also calculated for different signal models by varying the SNR,  $TE$ , and  $TE_{max}$  of the UTE-A sequence (see Figure 1) as done in simulations and phantom experiments. For obtaining different SNR levels, images were reconstructed with 1 and 2 averages by extracting data from the saved raw data files.  $TE$  and  $TE_{max}$  were varied by removing images with certain TEs from the entire echo train. Mean ( $\pm$ SD)  $R2^*$  values were measured by manual selection of an ROI covering the whole

liver cross-section and exclusion of blood vessels based on histogram analysis.<sup>18,19</sup> For each patient, the same ROI mask was used to calculate mean liver R2\* values for different signal models and acquisition parameters. For each fit, the mean R2\* values calculated by changing different UTE-A acquisition parameters were compared to those obtained with the 3-average UTE-A reference sequence.

### Statistical Analysis

The precision in R2\* estimation was evaluated using the coefficient of variation (CoV) plotted against true R2\* values. The accuracy in R2\* estimation was evaluated by calculating the relative error (in %) and by using linear regression analysis against reference R2\* values. For all statistical tests, p-values < 0.05 were considered significant.

## RESULTS

### Simulations

Precision of the R2\* estimates for all GRE acquisition methods (Fig. 2) showed an increase in CoV for R2\* values >1000 s<sup>-1</sup> except for GRE-A, which displayed lower precision for R2\* values <250 s<sup>-1</sup> compared to other GRE methods. Both UTE acquisitions demonstrated high precision for R2\* values >1000 s<sup>-1</sup>. UTE-A consistently produced high precision at all R2\* values above 50 s<sup>-1</sup>, whereas UTE-B exhibited an increase in CoV at decreasing R2\* values below 1000 s<sup>-1</sup>. With decreasing SNR, there was substantial loss of precision for all acquisition methods except for UTE-A.

The accuracy of R2\* estimates from reported acquisition methods with their respective fit models was variable (Fig. 3). GRE-A and GRE-C overestimated whereas GRE-B underestimated for R2\* values >1000 s<sup>-1</sup>, with error increasing with decreasing SNR. The UTE-A model using long TE<sub>max</sub> of 20.9 ms was accurate over the entire R2\* range for all simulated SNR, whereas UTE-B was accurate for R2\* values >1000 s<sup>-1</sup>, and accuracy decreased for lower R2\* values below 1000 s<sup>-1</sup>. Further, R2\* overestimation with UTE-B increased with decreasing SNR (up to ~8%), whereas UTE-A was not affected (relative errors <1%).

Figures 4 and 5 show R2\* accuracy and precision calculations for the 3 signal models (constant offset, noise subtraction, and quadratic mono-exponential) by varying UTE acquisition parameters. In both figures, R2\* values calculated with the UTE-A acquisition were taken as reference for all signal models for comparison, because this method had the highest precision and accuracy in R2\* measurements over the entire clinical R2\* range of 25 – 2000 s<sup>-1</sup> (see Figs. 2 and 3). Figure 4 shows that the noise subtraction and quadratic models had high accuracy for all SNRs whereas the constant offset model slightly overestimated R2\* (< 5%) for high SNRs (> 75); for the lowest SNR of 25, the constant offset model overestimated up to ~10%. All models showed similar precision for all SNRs, except that the CoV increased up to 10% for the lowest SNR (Fig. 5). All signal models had similar accuracy and precision for shorter TEs (0.25, 0.5 ms); however, accuracy and precision reduced for R2\* values above 1000 s<sup>-1</sup> using larger TEs (> 1ms). For the noise subtraction and quadratic models, decreasing TE<sub>max</sub> did not affect the accuracy of R2\*

estimates but increased the CoV for  $R2^*$  values  $<500 \text{ s}^{-1}$ . The effect of  $TE_{\max}$  was different in the constant offset model: for shorter  $TE_{\max}$ , there was overestimation and high CoV for  $R2^*$  values below  $500 \text{ s}^{-1}$ , and for longer  $TE_{\max}$  there was overestimation for  $R2^*$  values above  $500 \text{ s}^{-1}$  (Fig. 4).

### Phantom Study

The SNR in phantoms for the UTE-A acquisition ranged from 44 to 173 corresponding to the highest and lowest iron concentrations, respectively. All signal models produced similar  $R2^*$  results (Fig. 6) for different NAs and shorter TEs (0.25, 0.5 ms). However, using longer TEs  $\geq 1$  ms caused either  $R2^*$  underestimation or overestimation for all models at the highest iron concentration. Use of shorter or longer  $TE_{\max}$  produced similar  $R2^*$  results for the noise subtraction model at all iron concentrations. However, using shorter  $TE_{\max}$  (2.1, 4.7 ms) resulted in  $R2^*$  overestimation and high SDs for both the quadratic (relative errors up to  $\sim 130\%$  and CoVs up to  $\sim 45\%$ ) and constant offset (relative errors up to  $\sim 1600\%$  and CoVs up to  $\sim 130\%$ ) models at low iron concentrations ( $R2^* < 150 \text{ s}^{-1}$ ).

### In vivo Study

Figures 7 and 8 show the mean and CoV of  $R2^*$  values for different fits and acquisition parameters plotted against reference  $R2^*$  values. All signal models using UTE-A with 1 and 2 averages produced similar mean  $R2^*$  values as that by 3-average UTE-A acquisition (Table 2, slopes: 0.99–1.05,  $R^2 > 0.99$ ,  $P < 0.001$ ), except that the CoV was slightly higher for 1-average UTE-A acquisition. For all models, mean  $R2^*$  values and CoVs were similar between acquisitions with TEs of 0.25 and 0.5 ms. Increasing TE to 1 ms still produced similar mean  $R2^*$  results for all models (Table 2, slopes: 1.01–1.07,  $R^2: 0.98–0.99$ ,  $P < 0.001$ ) but increased the CoV in  $R2^*$  measurements to up to  $\sim 80\%$  for  $R2^*$  values above  $1000 \text{ s}^{-1}$  (Fig. 8). For a TE of 1.8 ms (minimum echo spacing possible with no interleaves in UTE-A acquisition), the constant offset and quadratic models systematically overestimated  $R2^*$  values and yielded high CoVs for cases of high iron ( $R2^* > 1000 \text{ s}^{-1}$ ), whereas the noise subtraction model underestimated  $R2^*$  values. In accordance with the phantom experiments, the noise subtraction model produced comparable mean  $R2^*$  results (Table 2, slopes: 1.02–1.06,  $R^2: > 0.99$ ,  $P < 0.001$ ) for short and long  $TE_{\max}$  over the entire  $R2^*$  range. However, for both the quadratic and constant offset models, using shorter  $TE_{\max}$  (2.1, 4.7 ms) overestimated  $R2^*$  and yielded high CoVs up to  $\sim 170\%$  for cases of mild iron ( $R2^* < 250 \text{ s}^{-1}$ ).

## DISCUSSION

In this study, the precision and accuracy of the main published biopsy calibrated  $R2^*$  acquisition and fitting methods, were assessed and compared with recently published UTE methods via simulations, phantoms, and *in vivo* data. While there are other  $R2^*$  acquisition methods and fitting algorithms currently tested (e.g. 3D-GRE and fat-corrected complex fitting), we focused on the calibration methods only, since these are the standard methods used in clinical practice where HIC in mg Fe/g tissue rather than  $R2^*$  values are reported and used by hematologists for excess iron removal therapy (e.g., chelation). Our findings indicate that the UTE with a longer  $TE_{\max}$  ( $\geq 10.1$  ms) and echo spacing of TE  $\geq 0.5$  ms is

the best among the investigated acquisition methods for reliable  $R2^*$  assessment over the entire clinical HIC range (0.2 to 60 mg/g Fe of dry weight liver tissue), and can be achieved within a reasonable scan time of only 1 to 1.5 minutes for 3 to 5 interleaves, respectively. Of all  $R2^*$  fitting models, the noise subtraction model was most robust to changes in UTE acquisition parameters and had higher accuracy and precision in  $R2^*$  measurements than the other fitting models.

The standard sequence used in published  $R2^*$ -MRI versus HIC by biopsy calibrations is a multi-echo GRE. However, previous studies and our numerical simulations show that current GRE techniques lose precision for  $R2^* > 1000 \text{ s}^{-1}$  (i.e., HIC  $> 25 \text{ mg Fe/g}$  at 1.5T),<sup>7,8</sup> except for GRE-A at high SNR. This is because GRE-A used multiple single-echo GRE acquisitions with larger voxel size that yielded relatively short  $TE_1$  and  $TEs$  than those by other GRE methods. However, GRE-A does not collect images with longer  $TEs$  ( $TE_{\max} = 4.8 \text{ ms}$ ) which leads to low precision for  $R2^*$  values  $< 250 \text{ s}^{-1}$  compared to other GRE methods. At low SNRs, all GRE acquisitions tested showed diminished precision for  $R2^*$  values even above  $500 \text{ s}^{-1}$  (i.e., HIC  $> 15 \text{ mg Fe/g}$ ). This limitation of conventional GRE imaging was more pronounced at 3T, as  $R2^*$  is approximately double that at 1.5T, which limits the maximal clinically measurable HIC to 12.5 mg Fe/g or even lower.

Limitations associated with GRE techniques at high HIC values or low SNR conditions may be overcome by using multi-echo UTE sequences.<sup>11,12</sup> Of the 2 published UTE acquisitions proposed for HIC assessment, our simulations showed that UTE-A provides high accuracy and precision over the entire  $R2^*$  range, whereas UTE-B was accurate and precise only at high  $R2^*$  values ( $> 1000 \text{ s}^{-1}$ ), apparently due to the use of a much shorter  $TE_{\max}$ . This means that UTE-B must be used in conjunction with a regular GRE sequence to cover the full clinical range of  $R2^*$  values with adequate accuracy and precision. Such a 2-tier imaging approach is viable in current clinical practice. A patient referred for iron assessment may always receive the GRE-based assessment first, thereby building on the vast diagnostic experience collected over the past decade. A UTE-B scan would then serve as a backup for failed GRE scans. However, for consistency, workflow optimization and to reduce patient burden, a single test covering the entire clinical range of  $R2^*$  values, such as UTE-A, is desirable.

As for  $R2^*$  fitting, our UTE simulations showed high accuracy and precision of  $R2^*$  measurements for all SNRs and signal models, except that the constant offset model overestimated  $R2^*$  by  $\sim 10\%$  at the lowest SNR levels, which is consistent with findings from previous studies.<sup>13,20</sup> In phantoms and *in vivo*, all signal models produced similar  $R2^*$  values for different number of averages indicating that UTE with 1-average is sufficient to obtain accurate results for  $25 < R2^* < 2000 \text{ s}^{-1}$ . In all experiments, the use of shorter  $TEs$  (0.25, 0.5 ms) gave similar accuracy and precision; however,  $R2^*$  accuracy and precision worsened at high  $R2^*$  values above  $1000 \text{ s}^{-1}$  for longer  $TEs$  1ms due to inadequate temporal sampling of the rapid signal decay. In phantoms and *in vivo*, using shorter or longer  $TE_{\max}$  produced similar  $R2^*$  results for the noise subtraction model across the entire  $R2^*$  range. However, using a shorter  $TE_{\max}$  led to  $R2^*$  overestimation and high SDs for both the quadratic and constant offset models in the low  $R2^*$  range ( $< 250 \text{ s}^{-1}$ ). This is because both quadratic and constant offset models fit a mono-exponential decay with an additional

parameter to account for noise floor. However, in cases of normal or mild iron overload, there is a gradual signal decay and with a shorter  $TE_{max}$  the signal does not hit the noise floor; thus, fitting a constant parameter for noise can yield inaccurate  $R2^*$  values. In contrast, the noise subtraction model fits a pure mono-exponential decay after subtracting the background noise from the signal, and hence the results do not seem to be affected despite using shorter  $TE_{max}$  in cases of normal or low iron.

Another important advantage of UTE imaging is that it can be performed under free breathing, as it is intrinsically less sensitive to motion because of radial sampling.<sup>11</sup> A recent study validated that free-breathing UTE outperforms free-breathing GRE in sedated and breath-hold non-compliant patients, which makes it a viable alternative to breath-hold GRE for accurate  $R2^*$  quantification even under conditions of non-massive iron overload.<sup>21</sup> Hence, UTE imaging can extend the measurable  $R2^*$ -based HIC range and eliminate the need for breath-holding when assessing hepatic iron overload by  $R2^*$ -MRI. This will increase the clinical suitability of UTE acquisition for assessing iron overload in pediatric populations and patients who are unable to hold their breath.

There are some limitations in this study. First, the acquisition time was longer for our reference sequence, UTE-A (100 s) than UTE-B (35 s), mainly because UTE-B acquires multiple single-echo acquisitions leading to a much shorter overall echo train length compared to UTE-A (7 vs. 60 echoes, respectively). However, we showed that a longer echo train length, as used in UTE-A, is necessary for accurately measuring low to moderate  $R2^*$  values ( $<500\text{ s}^{-1}$ ). Accurate measurements of short  $R2^*$  values are needed for therapeutic decisions, e.g. consideration for chelation therapy ( $<3.2\text{ mg Fe/g}$ ) or maintenance of an optimal chelation range ( $3.2\text{ mg Fe/g} - 7\text{mg Fe/g}$ ).<sup>22</sup> Hence, to sample longer  $TE_{max}$ , we recommend that UTE-B could be implemented as a multi-echo acquisition, which would, however, increase the scan time of UTE-B and bring it closer to acquisition times of UTE-A.

Second, UTE-A is a 2D sequence providing data from a single transverse liver slice only. For whole liver coverage, multiple slices of the liver could be measured by either repeating the UTE-A sequence at multiple slice locations or implementing a 3D UTE sequence such as UTE-B. However, both strategies will substantially increase the total scan time. The value of whole liver coverage for HIC assessment is unknown, considering that all existing  $R2^*$ -HIC calibrations were derived for single-slice acquisitions,<sup>7,8</sup> and iron removal therapies in patients seem to be successfully guided by those HIC values.<sup>23</sup>

Third, the UTE-A sequence uses fat suppression pulses to reduce streaking artifacts arising from the bright subcutaneous fat; otherwise the streaking artifacts can distort the signal in the liver and cause  $R2^*$  bias.<sup>11</sup> Recent GRE studies have shown that application of fat suppression pulses in iron overloaded cases, even without fat, can lead to  $R2^*$  underestimation.<sup>17,24</sup> However, Krafft et al. reported that there were only minor differences in  $R2^*$  values due to application of fat suppression pulses in UTE imaging.<sup>11</sup>

Fourth, the optimal sequence among the 5 acquisition methods investigated was identified based on simulations only. Ideally, all simulations would need to be validated



experimentally. But this was not possible in this study because we did not have access to all sequences as some of these were implemented on different vendor platforms.

Further, this study investigated only 3 validated R2\* fitting algorithms based on magnitude data. While handling noise in complex-based signal models is more straightforward than magnitude-based,<sup>25</sup> the complex-based methods require additional B<sub>0</sub> field estimation, and are also not yet validated against biopsy HIC measurements. A potential drawback of the magnitude-based signal models investigated in this study is that they do not account for the presence of fat, which is a confounding factor for R2\* estimation. Complex-based multispectral fat water models have been proposed for simultaneous quantification of fat and iron.<sup>25</sup> However, a recent study showed that the fat-corrected complex based non-linear least squares (NLSQ) methods substantially overestimated both R2\* and fat fractions in severely iron overloaded patients (R2\* > 500 s<sup>-1</sup>) when compared to liver biopsy results as reference standard.<sup>26</sup> In another study, investigators applied complex fitting only without fat correction for R2\* > 500 s<sup>-1</sup> to avoid instability and bias.<sup>27</sup> Due to these ambiguities, and also, as all of our UTE phantom and *in vivo* data were acquired with fat-suppression, we did not investigate fat-corrected complex-based methods in this study. However, the presented simulations may be an ideal framework to carry out these investigations (i.e., magnitude vs. complex-based fits, fat-uncorrected vs. fat-corrected fits) in future studies

Lastly, the signal models investigated in this study do not account for the presence of inflammation, and fibrosis or cirrhosis, which might confound R2\* estimation. Only future prospective patient studies with biopsy evaluation could evaluate the impact of these potentially confounding factors.

In summary, in this study we have developed a simulation approach for evaluating accuracy and precision which can also be applied to any acquisition technique and signal model in order to select the most appropriate methods for R2\* assessment. These simulations allow to study the impact of TE<sub>min</sub>, TE<sub>max</sub>, TE and SNR on the precision and accuracy of the fit. Our study demonstrates that UTE acquisition might offer a one-stop solution for R2\* quantification instead of GRE, by extending the measurable R2\* range, and removing the necessity for breath-holding. We found in simulations, phantom investigations and through the analysis of 137 exams of iron overloaded patients, that the free breathing UTE-A in combination with the noise subtraction model is a very suited approach that strikes a balance between measurement time, precision and accuracy, workflow and patient comfort.

## Supplementary Material

Refer to Web version on PubMed Central for supplementary material.

## Acknowledgements:

The authors thank Gail Fortner, RN, for patient enrollment and Chris Goode, RT, for MRI data collection. The authors also thank Dr. Vani Shanker for scientific editing.

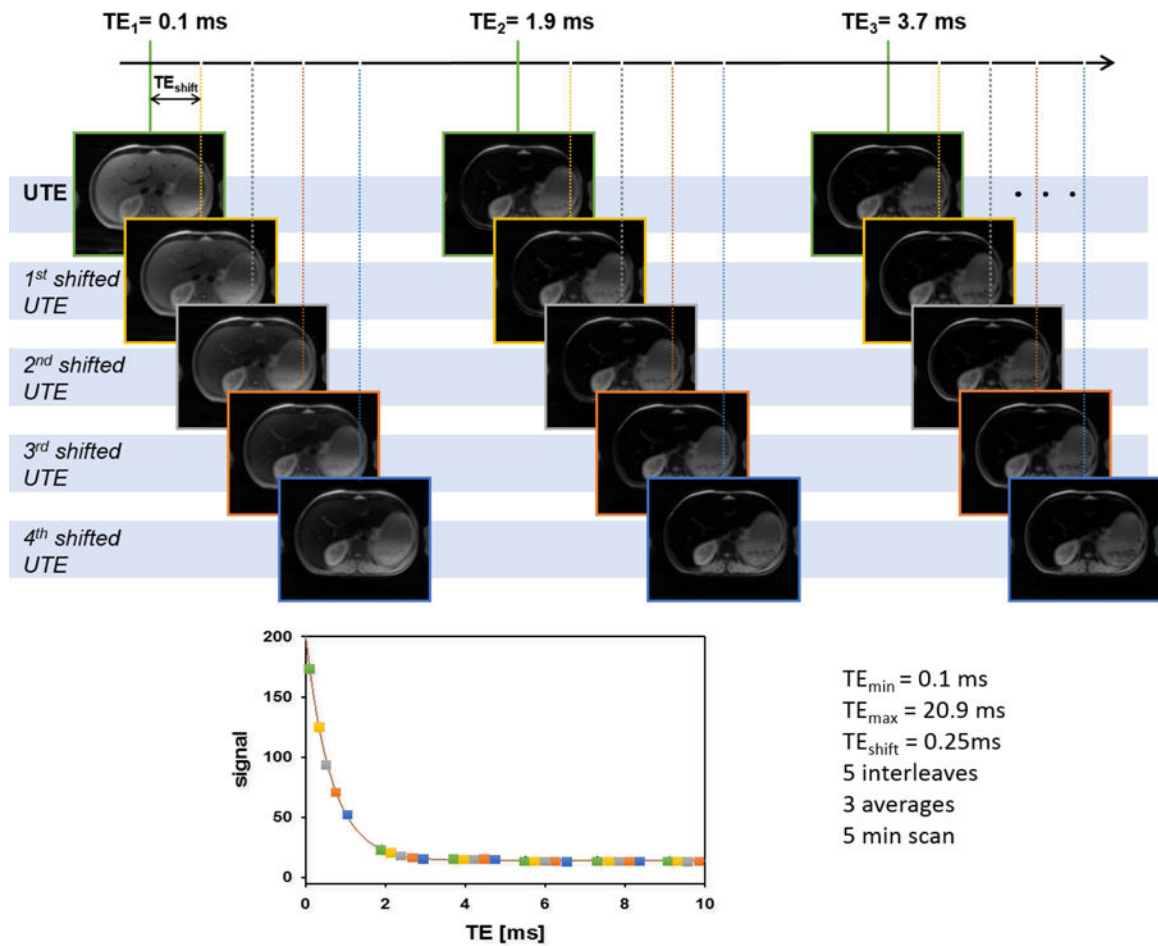
Grant Support:

This study was supported by grant 5 R01 DK088988 from the National Institute of Diabetes and Digestive and Kidney Diseases of the National Institutes of Health and by ALSAC (the fund-raising organization of St. Jude Children's Research Hospital).

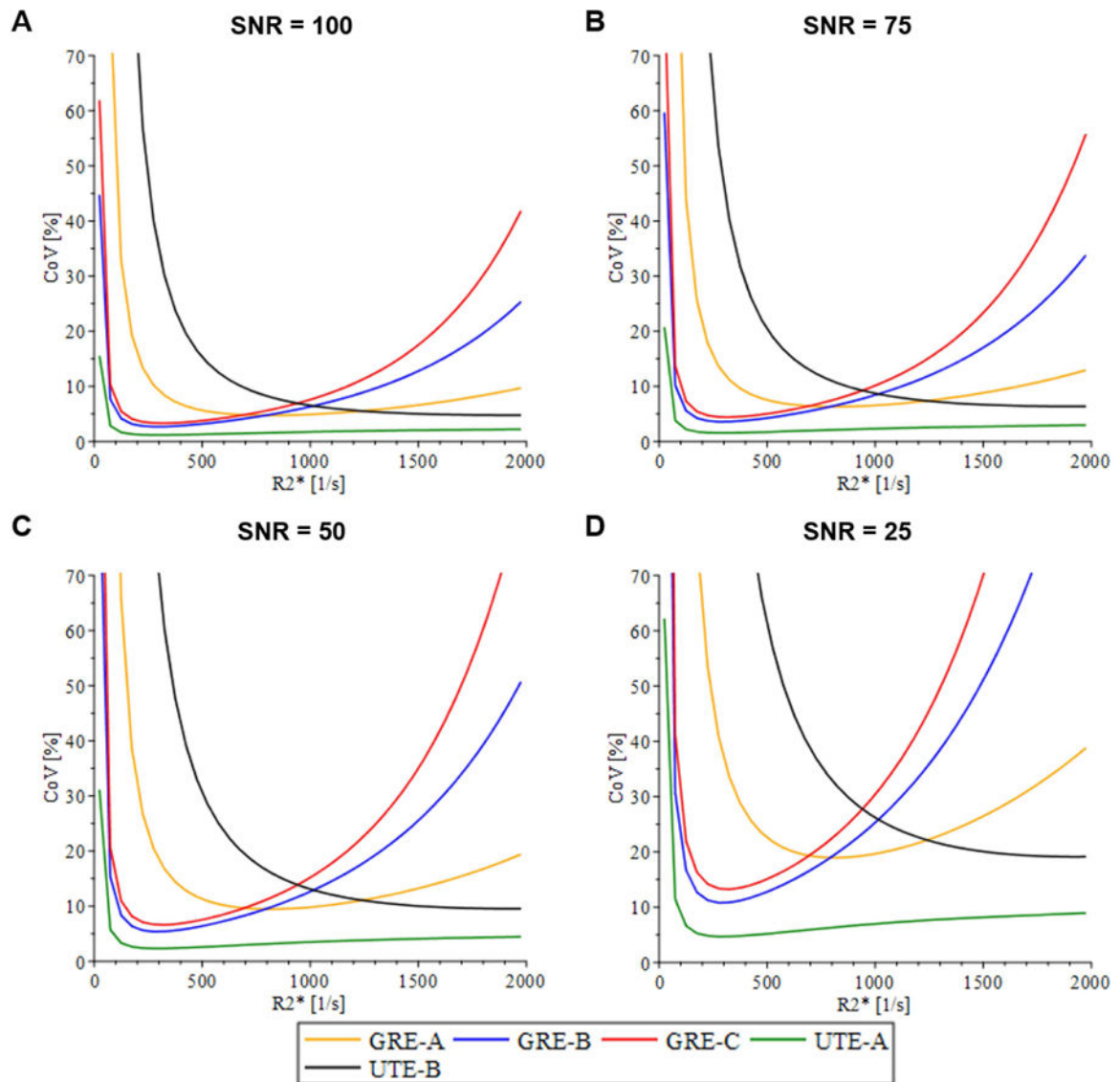
## REFERENCES

1. Olynyk JK, St Pierre TG, Britton RS, Brunt EM, Bacon BR. Duration of hepatic iron exposure increases the risk of significant fibrosis in hereditary hemochromatosis: a new role for magnetic resonance imaging. *The American journal of gastroenterology* 2005;100(4):837–841. [PubMed: 15784029]
2. Olivieri NF. Progression of iron overload in sickle cell disease. *Seminars in hematology* 2001;38(1 Suppl 1):57–62. [PubMed: 11206962]
3. Prati D, Maggioni M, Milani S, et al. Clinical and histological characterization of liver disease in patients with transfusion-dependent beta-thalassemia. A multicenter study of 117 cases. *Haematologica* 2004;89(10):1179–1186. [PubMed: 15477201]
4. Eng J, Fish JD. Insidious iron burden in pediatric patients with acute lymphoblastic leukemia. *Pediatric blood & cancer* 2011;56(3):368–371. [PubMed: 21072815]
5. Nottage K, Gurney JG, Smeltzer M, Castellanos M, Hudson MM, Hankins JS. Trends in transfusion burden among long-term survivors of childhood hematological malignancies. *Leukemia & lymphoma* 2013;54(8):1719–1723. [PubMed: 23163568]
6. Henninger B Demystifying liver iron concentration measurements with MRI. *European radiology* 2018.
7. Wood JC, Enriquez C, Ghugre N, et al. MRI R2 and R2\* mapping accurately estimates hepatic iron concentration in transfusion-dependent thalassemia and sickle cell disease patients. *Blood* 2005;106(4):1460–1465. [PubMed: 15860670]
8. Hankins JS, McCarville MB, Loeffler RB, et al. R2\* magnetic resonance imaging of the liver in patients with iron overload. *Blood* 2009;113(20):4853–4855. [PubMed: 19264677]
9. Garbowski MW, Carpenter JP, Smith G, et al. Biopsy-based calibration of T2\* magnetic resonance for estimation of liver iron concentration and comparison with R2 Ferriscan. *Journal of cardiovascular magnetic resonance : official journal of the Society for Cardiovascular Magnetic Resonance* 2014;16:40. [PubMed: 24915987]
10. Henninger B, Zoller H, Rauch S, et al. R2\* relaxometry for the quantification of hepatic iron overload: biopsy-based calibration and comparison with the literature. *RoFo : Fortschritte auf dem Gebiete der Röntgenstrahlen und der Nuklearmedizin* 2015;187(6):472–479. [PubMed: 25877992]
11. Krafft AJ, Loeffler RB, Song R, et al. Quantitative ultrashort echo time imaging for assessment of massive iron overload at 1.5 and 3 Tesla. *Magnetic resonance in medicine* 2017;78(5):1839–1851. [PubMed: 28090666]
12. Doyle EK, Toy K, Valdez B, Chia JM, Coates T, Wood JC. Ultra-short echo time images quantify high liver iron. *Magnetic resonance in medicine* 2018;79(3):1579–1585. [PubMed: 28643355]
13. Feng Y, He T, Gatehouse PD, et al. Improved MRI R2 \* relaxometry of iron-loaded liver with noise correction. *Magnetic resonance in medicine* 2013;70(6):1765–1774. [PubMed: 23359410]
14. Ogg RJ, Kingsley PB. Optimized precision of inversion-recovery T1 measurements for constrained scan time. *Magnetic resonance in medicine* 2004;51(3):625–630. [PubMed: 15004808]
15. Marquardt DW. An Algorithm for Least-Squares Estimation of Nonlinear Parameters. *Journal of the Society for Industrial and Applied Mathematics* 1963;11(2):431–441.
16. Press WH, Teukolsky SA, Vetterling WT, Flannery BP. *Numerical Recipes 3rd Edition: The Art of Scientific Computing*: Cambridge University Press: 2007 1256 p.
17. Krafft AJ, Loeffler RB, Song R, et al. Does fat suppression via chemically selective saturation affect R2\*-MRI for transfusional iron overload assessment? A clinical evaluation at 1.5T and 3T. *Magnetic resonance in medicine* 2016;76(2):591–601. [PubMed: 26308155]
18. McCarville MB, Hillenbrand CM, Loeffler RB, et al. Comparison of whole liver and small region-of-interest measurements of MRI liver R2\* in children with iron overload. *Pediatric radiology* 2010;40(8):1360–1367. [PubMed: 20333511]

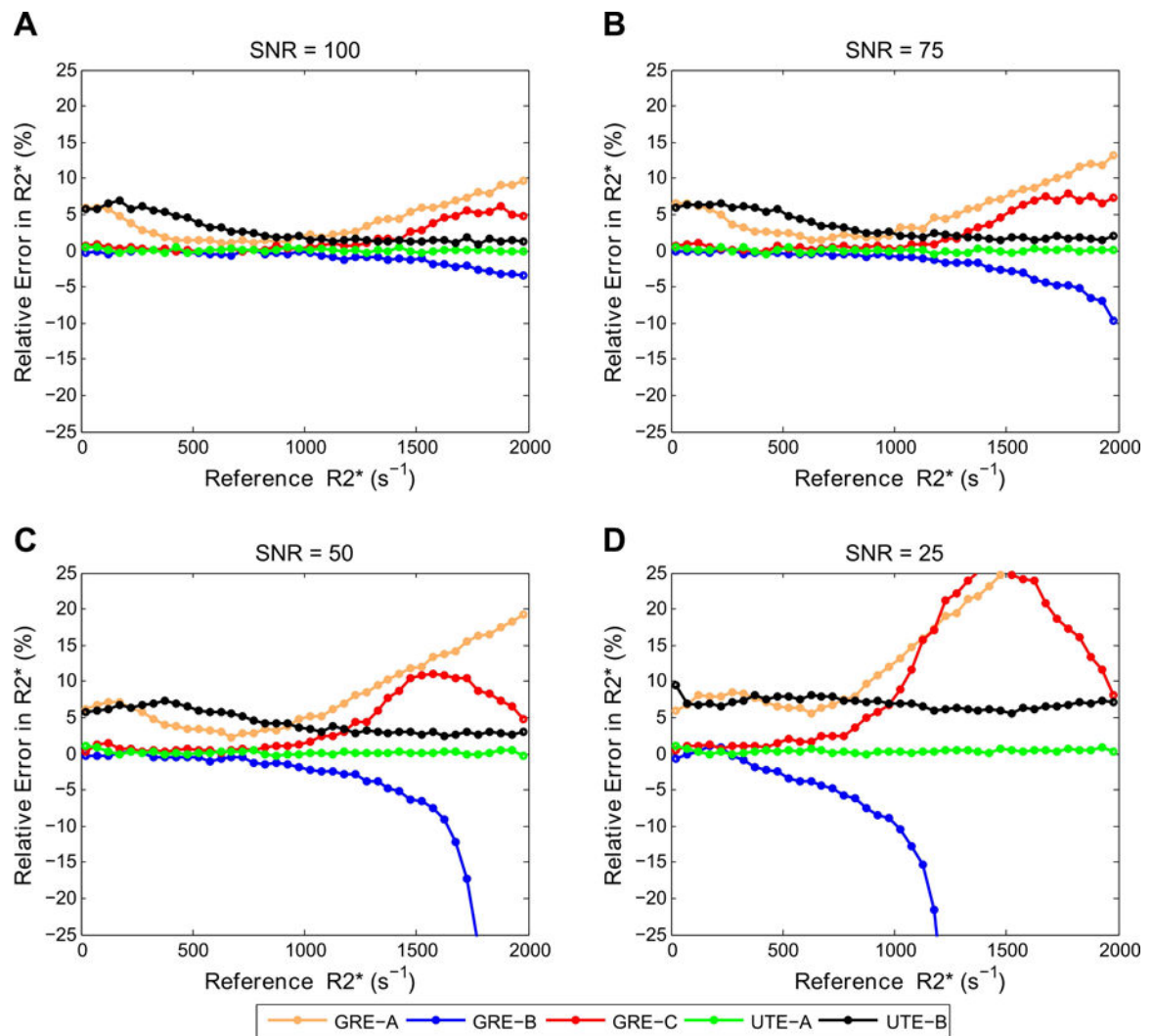
19. Deng J, Rigsby CK, Schoeneman S, Boylan E. A semiautomatic postprocessing of liver R2\* measurement for assessment of liver iron overload. *Magnetic resonance imaging* 2012;30(6):799–806. [PubMed: 22464453]
20. Yokoo T, Yuan Q, Senegas J, Wiethoff AJ, Pedrosa I. Quantitative R2\* MRI of the liver with rician noise models for evaluation of hepatic iron overload: Simulation, phantom, and early clinical experience. *Journal of magnetic resonance imaging : JMRI* 2015;42(6):1544–1559. [PubMed: 25996989]
21. Tipirneni-Sajja A, Krafft AJ, McCarville MB, et al. Radial Ultrashort TE Imaging Removes the Need for Breath-Holding in Hepatic Iron Overload Quantification by R2\* MRI. *AJR American journal of roentgenology* 2017;209(1):187–194. [PubMed: 28504544]
22. Olivieri NF, Brittenham GM. Iron-chelating therapy and the treatment of thalassemia. *Blood* 1997;89(3):739–761. [PubMed: 9028304]
23. Wood JC, Zhang P, Rienhoff H, Abi-Saab W, Neufeld E. R2 and R2\* are equally effective in evaluating chronic response to iron chelation. *American journal of hematology* 2014;89(5):505–508. [PubMed: 24452753]
24. Meloni A, Tyszka JM, Pepe A, Wood JC. Effect of inversion recovery fat suppression on hepatic R2\* quantitation in transfusional siderosis. *AJR American journal of roentgenology* 2015;204(3):625–629. [PubMed: 25714295]
25. Hernando D, Kramer JH, Reeder SB. Multiplex fat-corrected complex R2\* relaxometry: theory, optimization, and clinical validation. *Magnetic resonance in medicine* 2013;70(5):1319–1331. [PubMed: 23359327]
26. Tipirneni-Sajja A, Krafft AJ, Taylor BA, et al. Simultaneous Iron and Fat Quantification Using an Auto Regressive Moving Average Model at 1.5T and 3T. *Proceedings 25th Scientific Meeting, International Society for Magnetic Resonance in Medicine Honolulu, Hawaii; 2017 p. 326.*
27. Hernando D, Zhao R, Taviani V, et al. Liver R2\* as a Biomarker of Liver Iron Concentration: Interim Results from a Multi-Center, Multi-Vendor Reproducibility Study at 1.5T and 3T. *Proceedings 26th Scientific Meeting, International Society for Magnetic Resonance in Medicine Paris, France; 2018.*



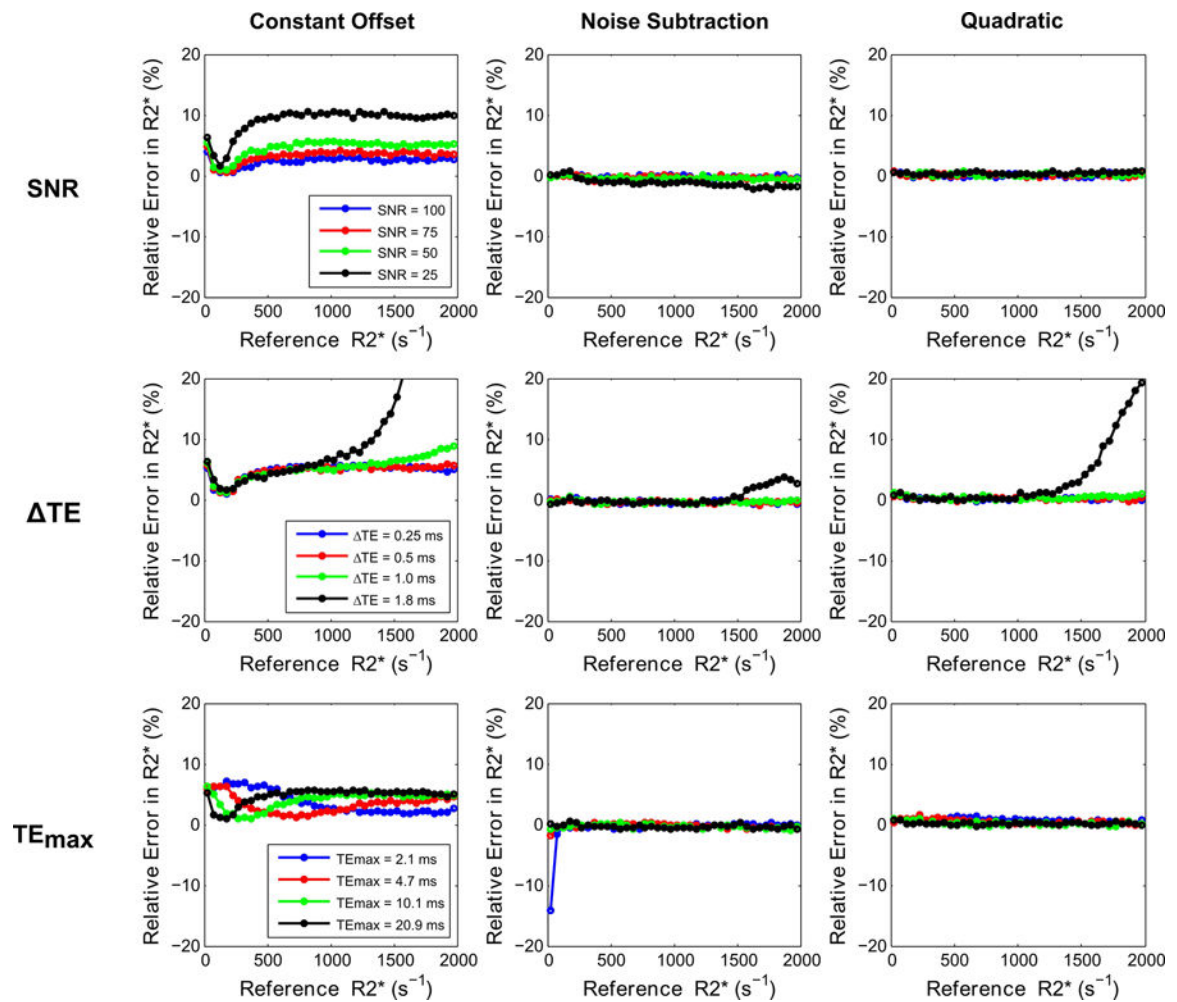
**FIG. 1.** Schematic description of the UTE-A acquisition with respective measurement parameters *in vivo*. The full data set is acquired in 5 interleaves, each interleave containing 12 echoes and shifted by  $TE_{\text{shift}} = 0.25$  ms from each other. The entire scan has been repeated 3 times to increase SNR. This results in a typical signal decay as shown in the bottom. Images acquired in each interleave are represented by a distinct color (green, yellow, grey, orange and blue). To study the impact of  $TE$  on accuracy and precision, every other echo (yellow & orange) has been removed. For investigation of the impact of  $TE_{\text{max}}$ , the last echoes have been sequentially removed to create echo trains with lengths of 60 (all data,  $TE_{\text{max}} = 20.9$  ms), 30 ( $TE_{\text{max}} = 10.1$  ms), 15 ( $TE_{\text{max}} = 4.7$  ms) and 7 ( $TE_{\text{max}} = 2.1$  ms). Finally, for SNR related simulations all 60 echoes and number of averages (NA) = 1, 2, 3 were used.

**FIG. 2.**

Coefficient of variance (CoV) plots for acquisition methods listed in Table 1, independent of the signal model under different signal-to-noise ratio (SNR) conditions. For high  $R2^*$  values ( $>1000 \text{ s}^{-1}$ ), all GRE acquisition methods had low precision whereas UTE acquisition methods had high precision. This demonstrates that  $TE_{\min}$  affects precision for the high  $R2^*$  range. In the low  $R2^*$  range, acquisitions that used longer  $TE_{\max}$  (GRE-B, GRE-C, UTE-A) had higher precision than did GRE-A and UTE-B, which used relatively much shorter  $TE_{\max}$ . This indicates that  $TE_{\max}$  affects precision for low  $R2^*$  values. As SNR decreased, all acquisitions showed a decrease in precision, indicating that SNR affects the overall precision.

**FIG. 3.**

Comparison of relative error in R2\* measurements for GRE and UTE methods listed in Table 1, using their respective fit models. For high R2\* values, GRE-A and GRE-C overestimated whereas GRE-B underestimated R2\* values, with underestimation or overestimation increasing with decreasing SNR. UTE-A showed the highest accuracy over the entire R2\* range for all SNRs, whereas UTE-B was accurate only for high R2\* and SNR.

**FIG. 4.**

Comparison of relative error in  $R2^*$  measurements (i.e., accuracy) for 3 signal models by varying UTE-A acquisition parameters as a function of SNR (top row),  $\Delta TE$  (middle row), and  $TE_{\max}$  (bottom row). SNR was held at 50 for varying  $\Delta TE$  and  $TE_{\max}$ . Noise subtraction and quadratic models showed high accuracy for varying acquisition parameters, except for high  $R2^*$  values obtained for the longest  $\Delta TE$  of 1.8 ms. The constant offset model overestimated  $R2^*$  for the lowest SNR and for high  $R2^*$  values obtained using longer  $\Delta TE$ s ( $> 1$ ms), and  $R2^*$  results were dependent on  $TE_{\max}$ .

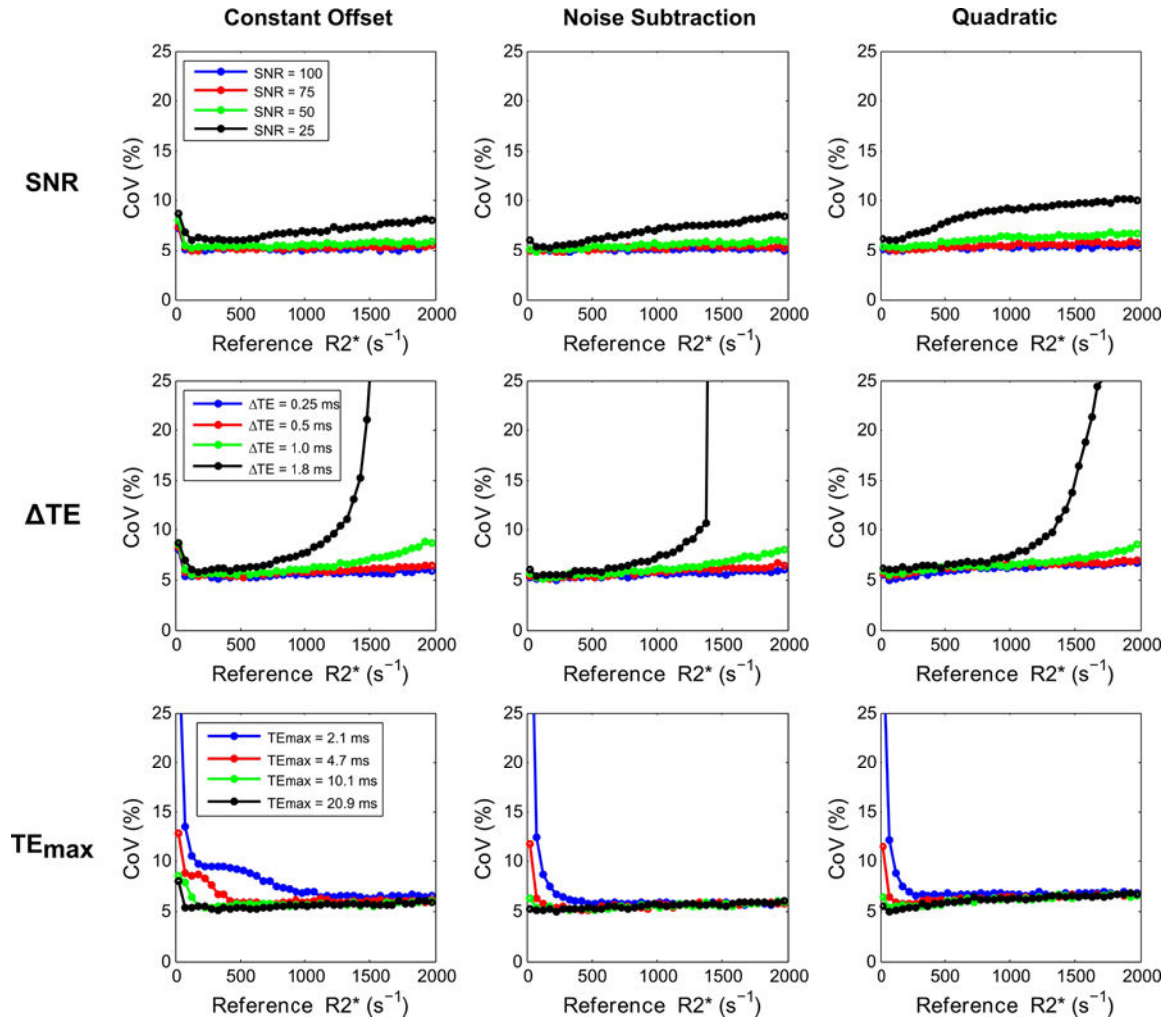


**FIG. 5.** Comparison of CoV in R2\* measurements (i.e., precision) for 3 signal models by varying UTE acquisition parameters as a function of SNR (top row), TE (middle row), and TE<sub>max</sub> (bottom row). SNR was held at 50 while varying TE and TE<sub>max</sub>. All models showed low precision for the lowest SNR, for high R2\* values obtained using longer TEs (1ms), and for low R2\* values obtained using shorter TE<sub>max</sub> (2.1, 4.7 ms).



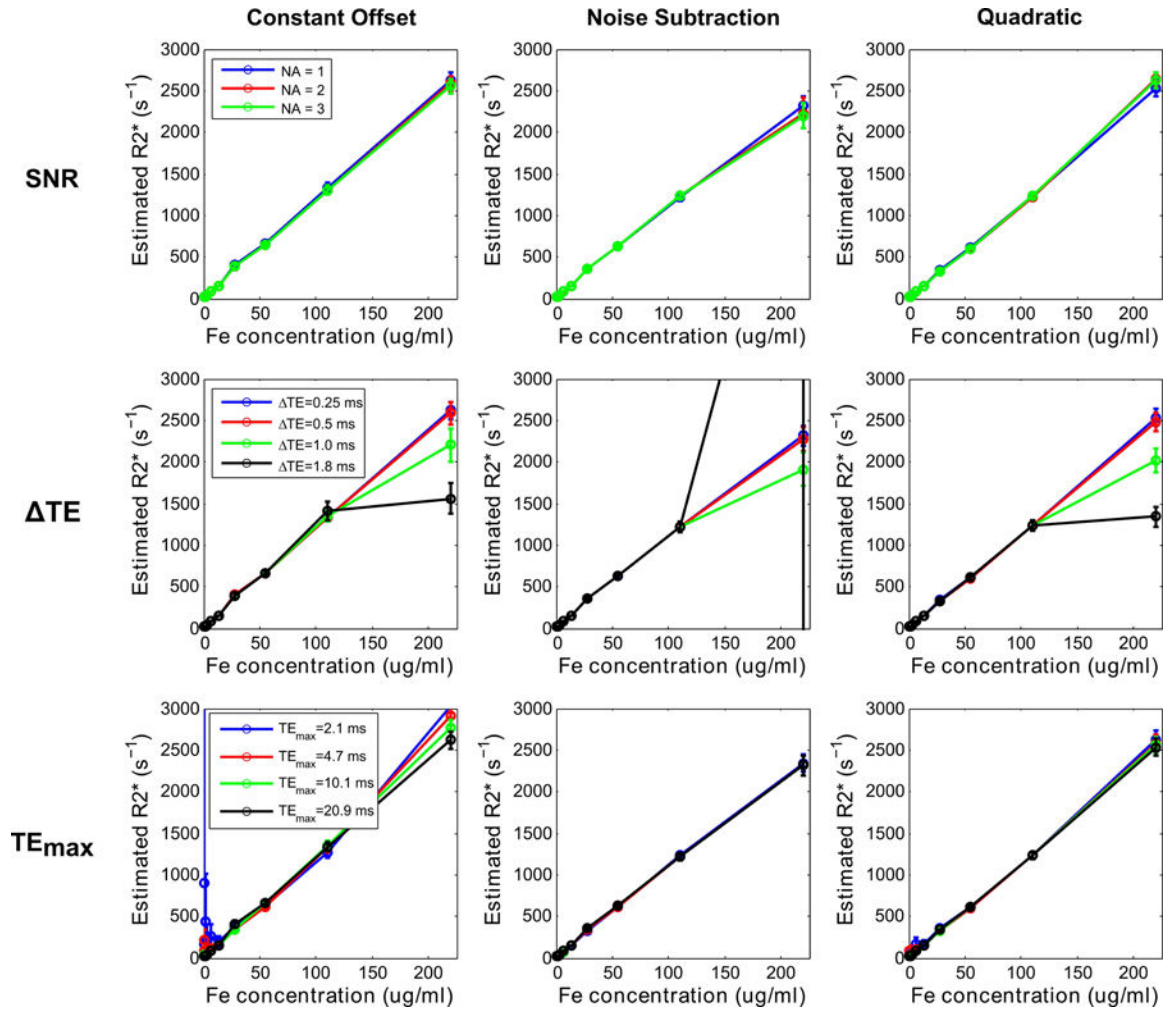


**FIG. 6.** Mean R2\* values (error bars denote standard deviation) obtained using 3 signal models plotted against iron concentrations in phantoms. UTE-A acquisition was taken as the reference, and parameters: SNR (top row), TE (middle row), and TE<sub>max</sub> (bottom row) were varied. SNR was compared by varying the number of averages (NA). All models produced similar R2\* values for different NA and underestimated or overestimated R2\* for the highest iron concentration obtained using longer TEs (1ms). For low iron concentrations and shorter TE<sub>max</sub> (2.1, 4.7ms), the constant offset model substantially overestimated R2\* values, the quadratic model only slightly overestimated, whereas the noise subtraction model still produced accurate results.

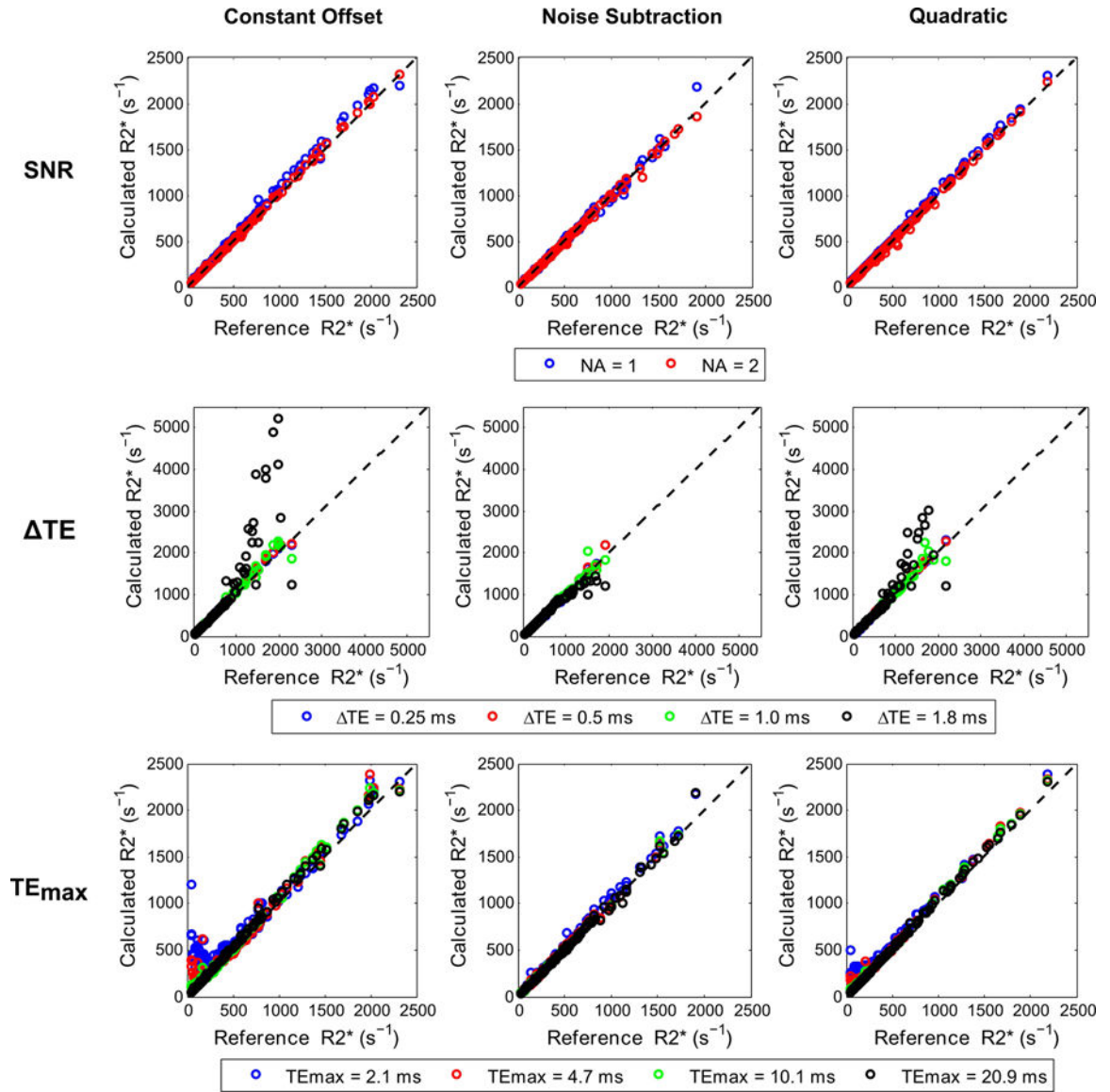


**FIG. 7.**

Mean  $R2^*$  values calculated with different fits by varying UTE-A parameters for *in vivo* data. For each fit, the mean  $R2^*$  values calculated by varying SNR (top row), TE (middle row), and  $TE_{max}$  (bottom row) were compared with those obtained using the 3-average UTE-A acquisition as reference. SNR was compared by varying the number of averages (NA). All models produced similar  $R2^*$  values for different NA and shorter TEs (0.25, 0.5 ms), but underestimated or overestimated  $R2^*$  for longer TEs ( $\geq 1$  ms) in cases of high iron overload ( $R2^* > 1000 \text{ s}^{-1}$ ). By using shorter  $TE_{max}$  (2.1, 4.7ms), the constant offset and quadratic models overestimated  $R2^*$  in cases of mild iron overload ( $R2^* < 250 \text{ s}^{-1}$ ) whereas the noise subtraction model still produced accurate results. Results of linear regression analysis (slope, intercept, and  $R^2$ ) between calculated and reference  $R2^*$  values for each fit are shown in Table 2.

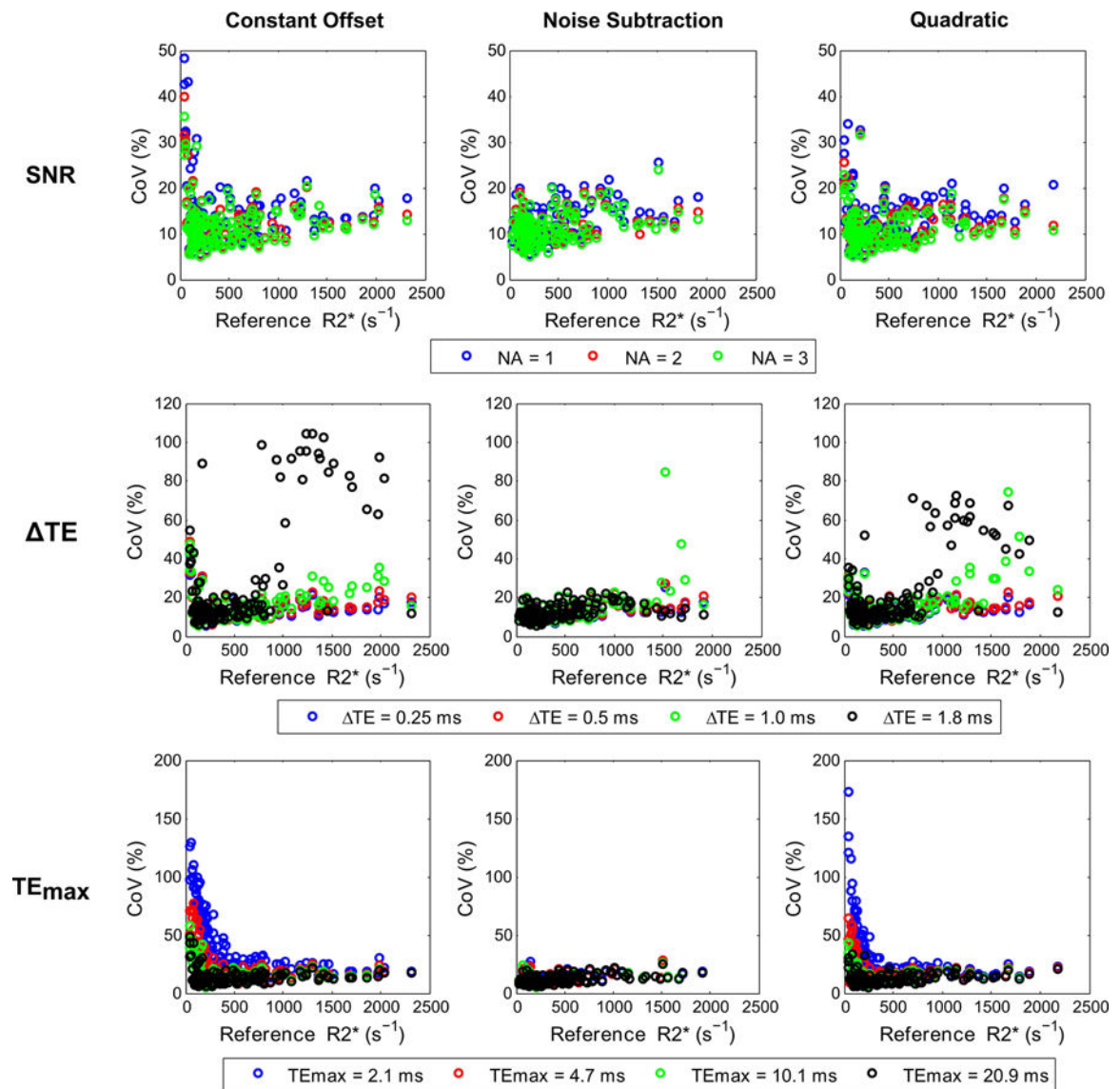


**FIG. 8.** Comparison of CoV in R2\* values calculated with different fits by varying UTE-A acquisition parameters: SNR (top row), TE (middle row), and TE<sub>max</sub> (bottom row). For each fit, the CoV of R2\* values are plotted against reference R2\* values calculated with the 3-average UTE-A acquisition. SNR was compared by varying the number of averages (NA). The CoV in R2\* values was similar for NA = 2, 3 but was slightly higher for NA = 1 for all model fits. Similarly, the CoV was similar for shorter TEs (0.25, 0.5 ms) but higher for longer TEs (1 ms) in cases of high iron overload (R2\* > 1000 s<sup>-1</sup>). Using longer TE<sub>max</sub> (10.1, 20.9 ms) yielded similar CoV in R2\* values for all models, but using shorter TE<sub>max</sub> (2.1, 4.7 ms) yielded high CoV in R2\* values for constant offset and quadratic models for cases of mild iron overload (R2\* < 250 s<sup>-1</sup>) whereas the noise subtraction model produced CoV similar to that using longer TE<sub>max</sub>.

**Table 1**

Summary of published R2\* Acquisition Methods and Signal Models

Method	TE <sub>min</sub> (ms)	TE <sub>max</sub> (ms)	TE (ms)	TR (ms) / FA(deg)	Slice thickness (mm)	FOV (mm)	Matrix	# Echoes	TA (min)	Signal Model	Reference
<b>GRE-A</b>	0.8	4.8	0.25	25/20	15	480	64×64	16	0:26	Mono-exponential with constant offset $S(t) = S_0 e^{-t \cdot R_2^*} + N$	Wood 2005 <sup>7</sup>
<b>GRE-B</b>	1.1	17.3	0.82	200/25	10	350–450	128×104	20	0:20	Mono-exponential with noise subtraction $S_{corr}(t) = \sqrt{(S(t))^2 - N^2}$ , $S_{corr}(t) = S_0 e^{-t \cdot R_2^*}$	Hankins 2009 <sup>8</sup>
<b>GRE-C</b>	0.93	15.66	1.34	20/20	10	320–384	128×96	12	0:15	Quadratic mono-exponential $S^2(t) = \left( S_0 e^{-t \cdot R_2^*} \right)^2 + N^2$	Feng 2013 <sup>13</sup>
<b>UTE-A</b>	0.1	20.9	0.25/0.8	52.5/20	10	350–500	192×192	60	1:40	Quadratic mono-exponential $S^2(t) = \left( S_0 e^{-t \cdot R_2^*} \right)^2 + N^2$	Krafft 2017 <sup>11</sup>
<b>UTE-B</b>	0.19	2.0	Variable (0.04 – 1.0)	5/4	15	310	88×88	7	0:35	Mono-exponential with constant offset $S(t) = S_0 e^{-t \cdot R_2^*} + N$	Doyle 2017 <sup>12</sup>

GRE, gradient echo; UTE, ultra-short echo time; TE<sub>min</sub>, minimum echo time; TE<sub>max</sub>, maximum echo time; TE, echo spacing; TR, repetition time; FA, flip angle; FOV, field of view; TA, acquisition time; S(t), measured signal; N, noise; S<sub>0</sub>, signal at the start of the decay; S<sub>corr</sub>(t), corrected signal after noise subtraction.

**Table 2**

Linear Regression Analysis between Calculated and Reference  $R2^*$  Values (in  $s^{-1}$ ) for Different Signal Models and UTE-A Acquisition Parameters for *In Vivo* Data.

Signal Model	Parameters	SNR			TE (ms)				TE <sub>max</sub> (ms)		
		NA = 1	NA = 2	0.25	0.5	1.0	1.8	2.1	4.7	10.1	20.9
Constant Offset	Slope	1.05	1.02	1.05	1.06	1.07	1.8	0.87	1.01	1.06	1.05
	Intercept	2.5	-1.9	2.5	-0.28	-1.6	-207	216	53	0.31	2.5
	$R^2$	>0.99	>0.99	>0.99	>0.99	0.99	0.80	0.90	0.97	>0.99	>0.99
Noise Subtraction	Slope	1.02	0.99	1.02	1.03	1.01	0.84	1.06	1.02	1.02	1.02
	Intercept	-4.8	1.5	-4.8	-6.2	-0.47	51	-1.1	0.25	-4.5	-4.8
	$R^2$	>0.99	>0.99	>0.99	>0.99	0.99	0.96	>0.99	>0.99	>0.99	>0.99
Quadratic	Slope	1.05	1.01	1.05	1.04	1.04	1.29	0.99	1.03	1.05	1.05
	Intercept	-4.2	-5.1	-4.2	-3.2	-1.9	-64	80	23	-1.0	-4.2
	$R^2$	>0.99	>0.99	>0.99	>0.99	0.98	0.87	0.98	>0.99	>0.99	>0.99

SNR, signal-to-noise ratio; NA, number of averages; TE, echo spacing; TE<sub>max</sub>, maximum echo time. P-value < 0.001 for all comparisons.